
WARP-LCA: Efficient Convolutional Sparse Coding with Locally Competitive Algorithm

Geoffrey Kasenbacher

Mercedes-Benz AG

Böblingen

Germany

geoffrey.kasenbacher@mercedes-benz.com

Felix Ehret

Mercedes-Benz AG

Böblingen

Germany

felix.ehret@mercedes-benz.com

Gerrit Ecke

Mercedes-Benz AG

Böblingen

Germany

gerrit.ecke@mercedes-benz.com

Sebastian Otte

Institut für Robotik und Kognitive Systeme

Universität zu Lübeck

sebastian.otte@uni-luebeck.de

Abstract

The locally competitive algorithm (LCA) can solve sparse coding problems across a wide range of use cases. Recently, convolution-based LCA approaches have been shown to be highly effective for enhancing robustness for image recognition tasks in vision pipelines. To additionally maximize representational sparsity, LCA with hard-thresholding can be applied. While this combination often yields very good solutions satisfying an ℓ_0 sparsity criterion, it comes with significant drawbacks for practical application: (i) LCA is very inefficient, typically requiring hundreds of optimization cycles for convergence; (ii) the use of a hard-thresholding results in a non-convex loss function, which might lead to suboptimal minima. To address these issues, we propose the Locally Competitive Algorithm with State Warm-up via Predictive Priming (WARP-LCA), which leverages a predictor network to provide a suitable initial guess of the LCA state based on the current input. Our approach significantly improves both convergence speed and the quality of solutions, while maintaining and even enhancing the overall strengths of LCA. We demonstrate that WARP-LCA converges faster by orders of magnitude and reaches better minima compared to conventional LCA. Moreover, the learned representations are more sparse and exhibit superior properties in terms of reconstruction and denoising quality as well as robustness when applied in deep recognition pipelines. Furthermore, we apply WARP-LCA to image denoising tasks, showcasing its robustness and practical effectiveness. Our findings confirm that the naive use of LCA with hard-thresholding results in suboptimal minima, whereas initializing LCA with a predictive guess results in better outcomes. This research advances the field of biologically inspired deep learning by providing a novel approach to convolutional sparse coding.

1 Introduction

Sparse coding has deep roots in neuroscience. The idea that sensory systems learn and represent the statistics of natural scenes date back to Barlow’s efficient coding hypothesis [Barlow et al., 1961]. Barlow reasoned that redundancy reduction is key, since information retrieval in the sensory stream is akin to finding the needle in the haystack. Sparse coding then originated from the insight that sparse, redundant representations may be useful to make the statistical components of sensory information explicit [Field, 1994, Barlow, 2001]. Within this context, the sparse coding algorithm, introduced by

[Olshausen and Field, 1996], has emerged as a paradigm to successfully model and predict response patterns of the primary visual cortex [Lee et al., 2006, 2007, Beyeler et al., 2019, Ecker et al., 2021].

The human cortex is a very homogeneous structure, and it has been hypothesized that it performs the same operation everywhere [Barlow, 1987]. The claim that sparse coding, at least to some degree, models general cortical function, reflects in a manifold of applications in which the algorithm has proven useful. It has early on been shown that the learned features are useful for inference [Rigamonti et al., 2011], especially when unsupervised learning can be leveraged, like in stereo vision [Lundquist et al., 2016, 2017, Ecker et al., 2021] or in scenarios with poorly labeled data [Zhang et al., 2017]. The capabilities for unsupervised learning are most prominent in multi layer sparse coding networks, which are capable of learning abstract concepts [Kim et al., 2018, Zhang et al., 2019, Dibbo et al., 2023]. In addition, sparse coding has proven at least state-of-the-art performance in removing noise and other corruptions from images [Lecouat et al., 2020]. More recently, Teti et al. [2022] has shown that applying sparse coding as a pre-processing stage in image recognition pipelines yields state-of-the-art robustness to common corruptions and adversarial attacks.

A significant challenge for applications with sparse coding is the computational expense of the inference algorithm. Finding sparse coefficients for each input sample requires an expensive iterative optimization process via gradient descent. One approach to resolve poor execution speed is the implementation on neuromorphic hardware. Rozell et al. [2008] introduced the Locally Competitive Algorithm (LCA) as a biologically plausible model for sparse coding. Indeed, the implementation of the LCA on Intel Loihi has proven the strongest gain in energy efficiency and execution speed against the implementation on conventional hardware, as compared to any other implemented algorithm [Davies et al., 2021, Henke et al., 2022, Parpart et al., 2023]. Considerable research has been directed towards developing efficient optimization algorithms for sparse coding on conventional hardware. Notable contributions include the works of Li and Osher [2009], Mairal et al. [2009], Beck and Teboulle [2009], and Vonesch and Unser [2007]. Gregor and LeCun [2010] contributed significantly to the field by introducing the Learned ISTA (LISTA) algorithm, which has spawned a family of model-based sparse encoders (notable models include AMP-Net Zhang et al. [2020], FISTA-Net Xiang et al. [2021] and ISTA-Net Zhang and Ghanem [2018]).

Sparse coding is typically associated with ℓ_1 norm regularization due to its convexity, which facilitates a tractable optimization process [Zhang et al., 2015]. However, for achieving maximum sparsity, ℓ_0 -like regularization is preferred [Paiton, 2019]. Despite its non-convex nature, which introduces computational challenges, ℓ_0 regularization directly targets sparsity in the solution [Nguyen et al., 2019]. Accelerated methods such as Learned Iterative Hard Thresholding (L-IHT) and Hard Thresholding Pursuit (HTP) have been developed to address ℓ_0 -like convergence problems. Nonetheless, the Locally Competitive Algorithm (LCA) presents a distinctive case. While the discrete version of LCA implementing ℓ_1 sparsity aligns mathematically with ISTA [Balavoine et al., 2015], employing an ℓ_0 -like cost function in LCA diverges significantly in outcomes when compared to greedy methods such as Basis Pursuit (BP) [Rozell et al., 2007, 2008].

Our main contribution of this paper is the development and validation of the Locally Competitive Algorithm with State Warm-up via Predictive Priming (WARP-LCA). This novel approach leverages a predictor network to provide an initial guess of the LCA state based on the current input, significantly improving convergence speed and solution quality. Specifically, WARP-LCA addresses the inefficiencies and suboptimal solutions associated with LCA using hard-thresholding (ℓ_0). By incorporating predictive priming, WARP-LCA dramatically reduces the number of optimization cycles required for convergence. Furthermore, WARP-LCA achieves superior minima, yielding more sparse and robust representations that enhance reconstruction and denoising quality, particularly in deep recognition pipelines. Our experiments, in the domain of image denoising and comparing WARP-LCA directly to LCA, confirm that WARP-LCA not only overcomes the limitations of traditional hard-thresholding LCA but also advances the field of biologically inspired deep learning by providing a novel and efficient method for convolutional sparse coding.

The remainder of this paper is structured as follows: Section 2 provides the background and related work, elaborating on convolutional sparse coding and the specifics of the Locally Competitive Algorithm. Section 3 details the WARP-LCA method, particularly focusing on the integration of the predictor network. In Section 4, we present our experimental setup and results, demonstrating the efficacy of WARP-LCA over traditional LCA in scenarios of image denoising and classification robustness. Section 5 discusses the broader implications of our findings and explores the general-

izability of WARP-LCA. Finally, Section 6 concludes the paper by summarizing our contributions and suggesting ways in which WARP-LCA could be applied to further applications and extended in future work.

2 Background and Related Work

2.1 Convolutional Sparse Coding

Convolutional sparse coding (CSC) is a technique used in signal processing and machine learning to learn a representation of data through the joint processes of inference and learning. The core idea is to represent input data using a sparse combination of basis functions.

Let the input image $x \in \mathbb{R}^{C \times H \times W}$ of height H and width W , with C channels, be represented by a learned overcomplete dictionary of convolutional features $\Phi \in \mathbb{R}^{M \times C \times k_H \times k_W}$, where M is the number of convolutional features, and k_H and k_W represent the spatial dimensions of each kernel. The input x can be represented as $x = \Phi \circledast a$, where \circledast denotes the transposed convolution operation and $a \in \mathbb{R}^{M \times \lfloor \frac{H}{\text{stride}_H} \rfloor \times \lfloor \frac{W}{\text{stride}_W} \rfloor}$ is the coefficient vector.

The inference process involves estimating the sparse coefficients a for a given data point x . This is typically achieved by minimizing an energy function that combines a reconstruction error term with a sparsity-inducing regularization term. A common formulation uses ℓ_p regularization to enforce sparsity [Tibshirani, 1996].

$$E(x, \Phi, a) = \|x - \Phi \circledast a\|_2^2 + \lambda \|a\|_p \quad (1)$$

Here, λ controls the strength of the sparsity constraint, balancing the trade-off between the reconstruction error and the sparsity of the coefficients. The choice of the sparsity criterion (i.e., the norm used for a) significantly affects the magnitude of the coefficients and the overall sparsity of the representation.

Learning in convolutional sparse coding involves updating the convolutional filters Φ based on the inferred sparse coefficients across a batch of data points. This is typically done through gradient descent on the energy function with respect to Φ . Although the joint optimization of Φ and a is non-convex, iterative approaches often converge to useful solutions, especially in natural signal domains. In addition to convolutional sparse coding, other widely known approaches for learning dictionaries include Principal Component Analysis (PCA) and Independent Component Analysis (ICA). PCA learns an orthogonal dictionary that captures the directions of maximum variance in the data. ICA, on the other hand, seeks to represent data as linear combinations of statistically independent components, which is useful for blind source separation and feature extraction [Hyvärinen and Oja, 2000].

2.2 Locally Competitive Algorithm (LCA)

The Locally Competitive Algorithm (LCA), introduced by Rozell et al. [2008], represents a biologically plausible approach to sparse coding, where the dynamics of the neuronal population can be conceptualized as a system of coupled differential equations that govern the temporal evolution of neuronal activities. Unlike iterative thresholding methods or matching pursuit, the LCA exhibits a 'charging circuit behavior' where neurons dynamically compete to represent the input.

To more intuitively describe the governing dynamics of the neurons in the context of Convolutional LCA, the states u_i and activations a_i refer to a map of neurons (neural map i), with the dimension $\frac{H}{\text{stride}_H}$ and $\frac{W}{\text{stride}_W}$, that correspond to a single kernel ϕ_i .

The dynamics of each neural map's membrane potential u_i follows the differential equation

$$\tau \frac{du_i}{dt} = -u_i + \phi_i * x + a_i - \sum_{i \neq j} a_j * (\phi_i * \phi_j), \quad (2)$$

Activations a_i are derived from a thresholding function applied to u_i :

$$a_i = T_\lambda(u_i). \quad (3)$$

where τ is a time constant that controls the rate of membrane potential decay. The self-inhibition term $-u_i$ dampens the dynamics, and the term $\phi_i * x$ represents the feedforward input to neural map i . The $+a_i$ eliminates self interaction from the following term. $\sum_{i \neq j} a_j * (\phi_i * \phi_j)$ couples the differential equations and can be seen as lateral competition between neural maps.

Rozell et al. [2008] introduced a generalized thresholding function that enables the Locally Competitive Algorithm (LCA) to tackle various sparse coding problems by adjusting its parameters. This function can interpolate between ℓ_1 and ℓ_0 regularization, providing a spectrum of sparsity constraints. The generalized thresholding function is expressed as:

$$T_\lambda(u_i) = \frac{u_i - \alpha\lambda}{1 + e^{-\gamma(u_i - \lambda)}} \quad (4)$$

In this equation, λ is a parameter that controls the sparsity level, α scales the threshold, and γ adjusts the steepness of the threshold function. By fine-tuning these parameters, the LCA can transition from soft-thresholding (promoting ℓ_1 sparsity) to hard-thresholding (promoting ℓ_0 sparsity).

Specifically, for ℓ_0 regularization—which aims to minimize the number of non-zero coefficients—the thresholding function approaches a hard threshold as γ becomes large. This effectively turns the generalized thresholding function into:

$$T_\lambda(u_i) = \begin{cases} u_i - \alpha\lambda, & \text{if } u_i > \lambda \\ 0, & \text{otherwise} \end{cases} \quad (5)$$

This hard-thresholding function enforces strict sparsity by zeroing out coefficients below the threshold λ , aligning with the goals of ℓ_0 regularization.

The initial values of the states in the LCA are typically set to zeros [Rozell et al., 2007], which can lead to slower convergence, especially under ℓ_0 constraints due to the non-convexity of the optimization landscape. This issue underscores the importance of effective initialization strategies to accelerate convergence when employing ℓ_0 regularization in LCA.

The LCA framework has demonstrated significant versatility in solving a range of sparse coding problems by appropriately setting the thresholding parameters. This adaptability makes the LCA a robust tool for sparse representation learning in diverse applications. Its major drawback, however, is that it becomes computationally intensive and slow when executed on standard computing hardware, particularly with ℓ_0 regularization, necessitating optimization techniques to improve its efficiency.

Recent implementations of the LCA on neuromorphic hardware have alleviated this problem to a certain extent by significantly enhancing the computational efficiency and execution speed by several orders of magnitude [Davies et al., 2021, Henke et al., 2022, Parpart et al., 2023]. Despite this progress, the algorithm still requires hundreds of optimization iterations and encounters substantial challenges with local optima. Thus, even with neuromorphic hardware, there is significant room for improvement in the underlying algorithmic principles.

2.3 Warm Starting with Deep Learning

A common approach to enhance the efficiency of iterative algorithms is to learn a mapping from problem parameters to high-quality initializations, known as warm starting. This technique leverages deep learning to predict an initial state that accelerates the convergence of iterative solvers.

Sambharya et al. [2023] introduced a framework for learning warm starts specifically for Douglas-Rachford splitting to solve convex quadratic programs (QPs), providing generalization guarantees for a broad range of operators. Similarly, Klaučo et al. [2019] used neural networks to warm-start active set methods in model predictive control (MPC), demonstrating significant reductions in computation time.

Beyond convex optimization, deep learning has been applied to accelerate non-convex optimization algorithms. For example, Sjölund and Bänkestad [2022] used graph neural networks to expedite matrix factorization, and developed schemes for quickly solving fixed-point problems. Inverse problems, such as sparse coding ([Gregor and LeCun, 2010], [Xin et al., 2016]), image restoration [Rick Chang et al., 2017], and wireless communication [He et al., 2020], have also benefited from

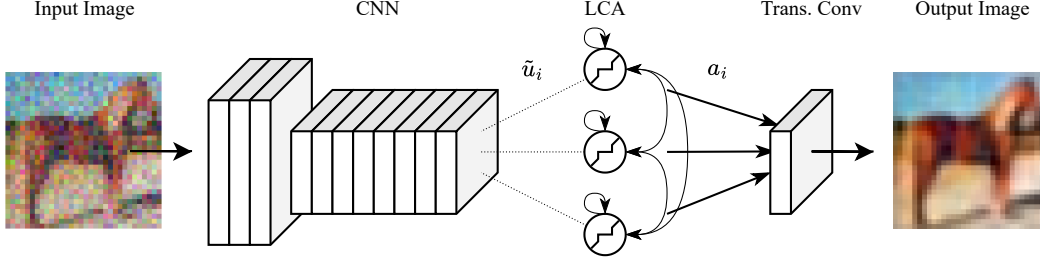


Figure 1: **Illustration of the WARP-LCA Method.** The WARP-LCA method integrates a fully convolutional neural network (CNN) to predict LCA states. These predicted states serve as a warm start for the LCA module. After several LCA iterations, the refined sparse activations are optionally processed through a transpose convolution block to reconstruct the image.

embedding algorithm steps into deep networks. A widely used technique is unrolling algorithmic steps, which differentiates through these steps to minimize a performance loss [Monga et al., 2021, Diamond et al., 2017, Gregor and LeCun, 2010].

3 WARP-LCA

Our approach introduces the **Locally Competitive Algorithm with State Warm-up via Predictive Priming (WARP-LCA)**, which integrates a predictor network into the traditional LCA framework. More specifically we propose a fully convolutional network for this purpose. The key contribution of our approach lies in the CNN’s role in predicting the initial states u_i for the LCA, facilitating faster convergence and enhancing the quality of the sparse code. Figure 1 shows a simple illustration of the approach.

The network is trained on internal states obtained from running the traditional LCA for many iterations and optionally for different sparsity levels. The sparsity level is encoded into the input data as an additional constant channel (i.e. $\text{RGB}\lambda$).

3.1 Predictor Network and Integration with LCA

The primary function of the predictor network is to provide an initial guess for the states u_i of the LCA, which are then refined through iterative optimization. This approach addresses the inefficiencies inherent in traditional LCA, which often requires numerous iterations to converge. Inspired by the findings of Xin et al. [2016], which demonstrate deep networks’ ability to recover minimal ℓ_0 -norm representations in high dimensional scenarios, our methodology strategically employs a predictive model to initialize the LCA.

Our network predicts the states u_i of the LCA rather than the activations a_i directly, a decision informed by empirical observations. You may find a detailed training procedure of WARP-LCA attached in the appendix C. Predicting activations, inherently sparse, resulted in suboptimal solutions, whereas predicting states, which typically exhibit no sparsity, proved more effective. The network effectively learns to predict a ‘mean’ sparse code—essentially the most probable sparse representation conditioned on the input. This is conceptualized as the network learning the conditional expectation $E[S|X] \approx f(X; \theta^*)$, where $f(X; \theta)$ maps an input X to an optimal state S , and θ^* are the optimized parameters.

This predictive initialization significantly enhances the LCA’s performance by positioning the algorithm near an (expected) optimal starting point in the solution space, as inferred from the training data. It not only accelerates convergence but also ensures that the resultant sparse representations are more robust, effectively bypassing poorer minima that the LCA alone might settle into. Thus, by leveraging the statistical regularities of sparse codes learned during training, the model not only speeds up the optimization process but also elevates the fidelity of the encoded features, contributing to both computational efficiency and enhanced solution quality.

Note that for this work we did not further explore the full range of possible CNN architecture for the predictor network, but settled on a trade-off between model complexity and effectiveness (see Table 4 for more details on the architecture). What we found in preliminary experiments, however, is that a subtractive ReLU arrangement as used in Lang et al. [2023], combining the computation branches in the network was necessary to balance sparsity and richness of the output:

$$u_i = \sigma(\text{relu}(a_i) - \text{relu}(b_i)) \quad (6)$$

where a_i and b_i are output of the computational paths of the architecture shown in Table 4 for a single kernel i and σ is the standard sigmoid function. This setup allows to establish a stable reference value that is neither the minimum nor the maximum and also the branches to specialize on the range above and below this reference value, respectively.

4 Experiments and Results

In our experiments we used the CIFAR-10 dataset [Krizhevsky et al., 2009] for learning both the dictionary and the encoder model (WARP-CNN). The dictionary was learned using a soft thresholding LCA approach (you may find the dictionary here Figure 6). Additionally, to test the versatility of our method on out-of-distribution data we employed the Oxford Pets dataset [Parkhi et al., 2012]. All of our experiments were conducted on a Linux system equipped with three NVIDIA Tesla V100-PCIE-16GB GPUs, each with a compute capability of 7.0 and 16.94 GB of memory. The system also features 8 CPU cores and memory resources, with a total of 201.18 GB of RAM and 174.20 GB available. On average, training took 15.6 iterations per second using batches of 32 images (for dictionary training on the CIFAR dataset, with 200 LCA iterations).

The primary task and comparison for our WARP-LCA model was against the traditional LCA method. This choice allowed for a direct evaluation of the enhancements offered by our predictive initialization approach under identical encoding conditions.

Performance was assessed using Mean Squared Error (MSE), ℓ_0 -norm, Peak Signal-to-Noise Ratio (PSNR), and Structural Similarity Index (SSIM). These metrics were chosen to provide a comprehensive view of both quantitative and qualitative measures. Each model was executed for 1,000 iterations with lambdas set at 0.15 and 0.85, alongside several intermediate levels to analyze relative speed improvements based on maximum PSNR achieved by the LCA after 1000 iterations. Execution of the models, i.e. inference allows us to change the number of iterations. To compare both WARP-LCA and LCA up to full convergence, we have evaluated inference after 1000 iterations.

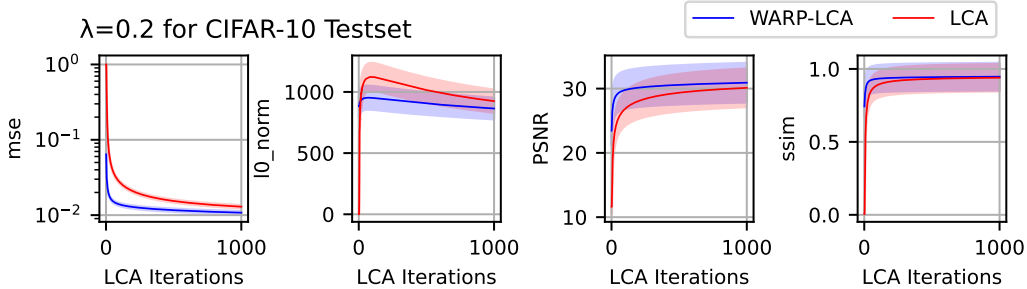


Figure 2: **Encoding Performance Comparison between WARP-LCA and LCA at $\lambda = 0.2$.** The figure displays the performance metrics for WARP-LCA and LCA. The columns represent different metrics: Log Mean Squared Error (MSE), ℓ_0 -Norm, Peak Signal-to-Noise Ratio (PSNR), and Structural Similarity Index (SSIM). For each plot, WARP-LCA and LCA Mean and Standard Deviation of the Metrics are shown for comparison.

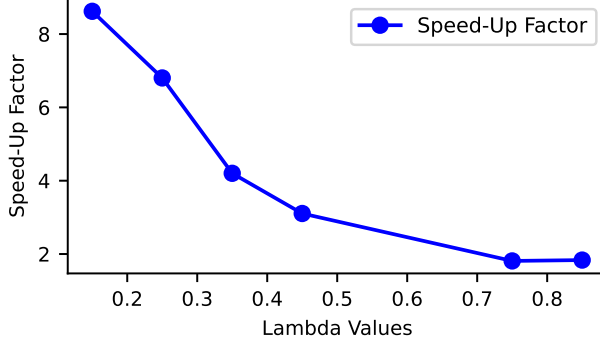


Figure 3: **Relative Speed Up of WARP-LCA Compared to LCA.** The graph quantifies the efficiency of WARP-LCA relative to LCA in achieving equivalent PSNR levels, using the CIFAR-10 test set for evaluation. The comparison point for PSNR is established after 1000 iterations of the LCA. The vertical axis depicts the reduction in the number of iterations required by WARP-LCA to match the PSNR achieved by LCA.

Table 1: Evaluation after 1000 iterations on CIFAR-10 dataset with $\lambda = 0.15$

Metric	WARP-LCA Metrics Mean	LCA Metrics Mean
Recon. MSE	0.0108	0.0129
L_0 Norm	864.62	924.81
L_1 Norm	466.86	422.34
PSNR	30.92	30.12
SSIM	0.9467	0.9398

Our results, presented in Figure 2 and in Table 1, highlight significant findings. The WARP-LCA demonstrated markedly faster convergence in terms of MSE as indicated by the $\log(\text{MSE})$ trajectory, maintaining a superior MSE even after 1,000 iterations compared to the standard LCA. Similarly, ℓ_0 -norm results showed that WARP-LCA began near optimal sparsity levels, whereas LCA required considerable iterations to approximate these levels. Markedly the ℓ_0 -norm achieved by the WARP-LCA is lower than ℓ_0 -norm reached by the LCA. Both PSNR and SSIM metrics reflected faster convergence and higher final values for the WARP-LCA.

4.1 Denoising Performance in Classification Pipelines

To evaluate the robustness of our WARP-LCA model in enhancing the denoising capabilities within classification pipelines, we employed three distinct pre-trained convolutional neural network architectures: DenseNet-40 with a growth rate of 12 on CIFAR-10 [Huang et al., 2017], Wide Residual Network with depth 40 and widening factor 8 on CIFAR-10 [Zagoruyko and Komodakis, 2016], and ResNeXt with 29 layers and cardinality 32 using 4d expansions [Xie et al., 2017].

The test set images from CIFAR-10 were subjected to varying levels of additive Gaussian noise. For each noise level and each backbone architecture, two denoising strategies were applied: traditional LCA-based denoising, run for 800 iterations, and our WARP-LCA-based denoising, run for 200 iterations. This approach allowed us to directly compare the efficacy of our WARP-LCA model against the standard LCA under identical noise conditions, consistent with earlier experiments demonstrating comparable PSNR values between the models. Although different levels of noise typically require adjustments to the sparsity parameter λ , we opted for a λ of 0.2 across all noise levels, drawing from methodologies similar to those reported by Teti et al. [2022]. Denoising performance was quantitatively assessed by measuring the classification accuracy post-denoising.

As shown in Figure 4, WARP-LCA consistently outperforms traditional LCA in terms of classification accuracy across all tested noise levels and models.

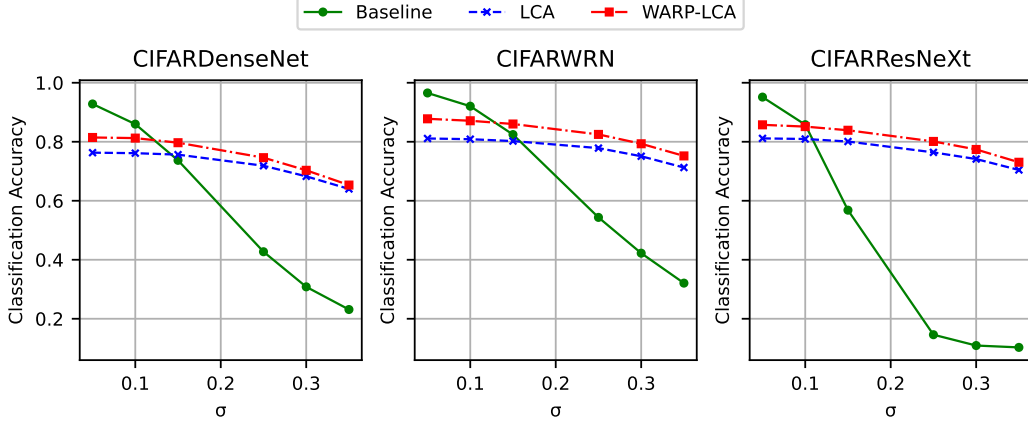


Figure 4: **Testing Robustness against Noise** The graph shows evaluations of CIFAR-10 on DenseNet, WideResnet and ResNext with WARP-LCA and LCA frontend for varying levels of additive gaussian noise (σ is the standard deviation).

5 Discussion

The comparative analysis in Section 4 (illustrated in Figure 2) compellingly demonstrates the superior efficacy of WARP-LCA, over the traditional LCA: faster convergence and settling for deeper minima. This attribute was consistently evident across a range of noise levels and architectural backbones in the denoising experiment in Section 4.1. These results not only corroborate but also extend the findings by Teti et al. [2022], propelling WARP-LCA beyond the current state-of-the-art. This advancement underscores the potential of predictive initializations to redefine performance benchmarks in the field, offering robust, fast, and more accurate sparse coding.

The robustness of WARP-LCA, particularly for out-of-distribution data, was tested on the Oxford Pets dataset [Parkhi et al., 2012], which starkly contrasts with CIFAR-10 in terms of image size (images in the Oxford Pets dataset are much larger) and image statistics. The Oxford Pets dataset is a collection of images featuring 37 different breeds of cats and dogs, each annotated with class labels, bounding boxes, and pixel-level segmentation masks. Despite these considerable differences, and the fact that our models were initially trained only on CIFAR images, the fully convolutional nature of predictor architectures allowed for an efficient adaptation to this new context.

The (relative) accumulated activation map generated by WARP-LCA provides more homogeneous and less extreme structures than the accumulated LCA activation map, indicated much more uniformly distributed activations. Even after 300 iterations, activity in the accumulated LCA map is still concentrated in very dark and light areas of the image. In addition, WARP-LCA also has a lower ℓ_0 -Norm than the LCA. The reconstructed image from the LCA appears not to have converged yet, as the colors, especially in the light and dark areas, seems to be faded. The reconstructed image from the WARP-LCA seems to be much closer to the original. This may imply that the CIFAR dictionary alone may be sufficient to be used on data other than CIFAR images and WARP-LCA managed to predict states that lead to a consistent and balanced activation profile.

We have experimented with different approaches to warm-starting LCA, including random initialization but found that the only methods that lead to convergence are the conventional zero initialization as is typical for LCA and our CNN predictor. We have compared the similarity of learned cifar10-kernels to the correlation of activations of LCA and WARP-LCA after 1000 optimization cycles up to convergence and found that the WARP-LCA method has lower correlation between kernels as would be expected from the earlier results. The prediction of initial states leads to more diverse and robust minima (please see the appendix for a comparison of LCA, WARP-LCA, CNN-only prediction and simple convolution).

During our exploration, we opted for a balance between model complexity and effectiveness, as detailed in Table 4. While we assessed performance at various sparsity levels, notably at $\lambda=0.85$,

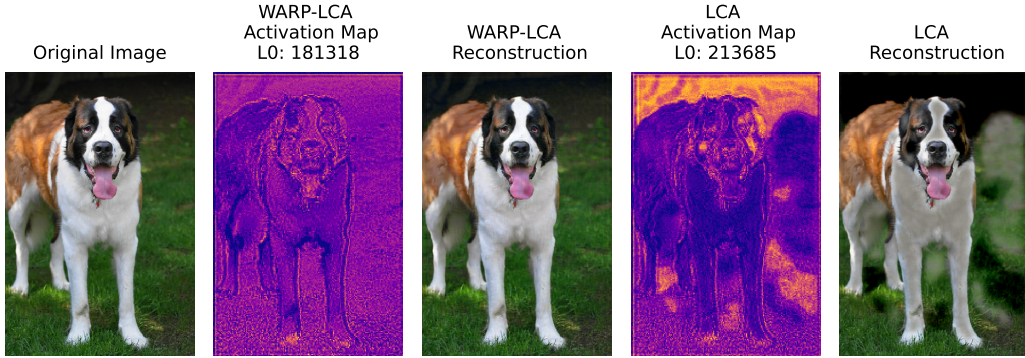


Figure 5: **Accumulated activation maps for WARP-LCA and LCA.** This figure presents the original image and the activation maps generated by WARP-LCA and LCA, with a sparsity level ($\lambda = 0.15$). Accumulated activation maps are computed as the count of non-zero sparse coefficients across different channels (normalized between 0 and 1 across both activation maps to highlight relative activation levels). The WARP-LCA map is derived after 10 iterations, whereas the LCA map results from 300 iterations.

the predictive performance of WARP-LCA diminished, as documented in the appendix. This reduction likely stems from the restricted solution space at higher sparsity levels, where fewer unique kernel combinations are viable for reconstructing the input. In contrast, at lower lambdas, it was possible to achieve minima that significantly outperformed traditional LCA.

It is important to note that our experiments were conducted using a single, learned over-complete dictionary. The application of WARP-LCA to dictionaries with lower overcompleteness—and hence fewer kernels—might prove more challenging. Yet, a larger dictionary typically enhances the benefits of WARP-CNN in terms of convergence and solution quality, as demonstrated in Figure 5. Unlike the approach by [Teti et al., 2022], we did not train the backbones on sparse activations but rather opted to reconstruct the image, which allowed us to employ pretrained backbones and evaluate WARP-LCA and LCA as distinct preprocessing modules. Training a classification model on sparse activations obtain by WARP-LCA may provide more robustness.

It should be noted as well that neither LCA nor WARP-LCA can reconstruct or fill missing areas beyond local disturbances with semantically useful information, since the principle does not provide top-down, that is, high-level and context-dependent projections, which is accomplished e.g. with generative models.

Looking forward, extending WARP-LCA to directly handle noisy inputs could considerably improve its practical applicability, particularly in scenarios where noise pervades. Additionally, developing adaptive models that can predict not only the initial states but also the optimal number of iterations and lambda may lead to promising results. Such advancements could lead to sparse coding systems that are more autonomous and efficient, effectively bridging the gap between theoretical constructs and their practical implementation.

6 Conclusion

This research introduces WARP-LCA, an enhanced version of the Locally Competitive Algorithm (LCA), and demonstrates its efficacy in terms of accelerating convergence, improving robustness, and enabling the algorithm to achieve deeper minima and hence better solutions. As compared to the original LCA, we consistently observed improvements of image reconstruction metrics across various noise levels, and improvements of noise robustness across several deep neural network backbone architectures.

Our investigations further revealed the robust generalizability of WARP-LCA, particularly with the Oxford Pets dataset, which significantly differed from the training dataset (CIFAR) in image size, type, and image statistics.

Looking ahead, expanding the capabilities of WARP-LCA to directly process noisy inputs could dramatically enhance its applicability for denoising, robustness, and other sparse coding applications.

References

- Aurele Balavoine, Christopher J Rozell, and Justin Romberg. Discrete and continuous-time soft-thresholding for dynamic signal recovery. *IEEE Transactions on Signal Processing*, 63(12): 3165–3176, 2015.
- Horace Barlow. Cerebral Cortex as Model Builder. In Lucia M. Vaina, editor, *Matters of Intelligence: Conceptual Structures in Cognitive Neuroscience*, pages 395–406. Springer Netherlands, Dordrecht, 1987. ISBN 978-94-009-3833-5. doi: 10.1007/978-94-009-3833-5_18. URL https://doi.org/10.1007/978-94-009-3833-5_18. Reporter: Matters of Intelligence: Conceptual Structures in Cognitive Neuroscience.
- Horace B Barlow. Redundancy reduction revisited. *Network: Computation in Neural Systems*, 12(3):241–253, January 2001. doi: 10.1080/net.12.3.241.253. URL <https://doi.org/10.1080/2Fnet.12.3.241.253>. Publisher: Informa UK Limited.
- Horace B Barlow et al. Possible principles underlying the transformation of sensory messages. *Sensory communication*, 1(01):217–233, 1961.
- Amir Beck and Marc Teboulle. A fast iterative shrinkage-thresholding algorithm for linear inverse problems. *SIAM Journal on Imaging Sciences*, 2(1):183–202, 2009.
- Michael Beyeler, Emily L Rounds, Kristofor D Carlson, Nikil Dutt, and Jeffrey L Krichmar. Neural correlates of sparse coding and dimensionality reduction. *PLoS computational biology*, 15(6): e1006908, 2019.
- Mike Davies, Andreas Wild, Garrick Orchard, Yulia Sandamirskaya, Gabriel A Fonseca Guerra, Prasad Joshi, Philipp Plank, and Sumedh R Risbud. Advancing neuromorphic computing with loihi: A survey of results and outlook. *Proceedings of the IEEE*, 109(5):911–934, 2021.
- Steven Diamond, Vincent Sitzmann, Felix Heide, and Gordon Wetzstein. Unrolled optimization with deep priors. *arXiv preprint arXiv:1705.08041*, 2017.
- Sayanton V Dibbo, Juston S Moore, Garrett T Kenyon, and Michael A Teti. Lcanets++: Robust audio classification using multi-layer neural networks with lateral competition. *arXiv preprint arXiv:2308.12882*, 2023.
- Gerrit A Ecke, Harald M Papp, and Hanspeter A Mallot. Exploitation of image statistics with sparse coding in the case of stereo vision. *Neural Networks*, 135:158–176, 2021.
- David J. Field. What Is the Goal of Sensory Coding? *Neural Computation*, 6(4):559–601, July 1994. doi: 10.1162/neco.1994.6.4.559. URL <https://doi.org/10.1162/2Fneco.1994.6.4.559>. Publisher: MIT Press - Journals.
- Karol Gregor and Yann LeCun. Learning fast approximations of sparse coding. *Proceedings of the 27th International Conference on Machine Learning (ICML-10)*, pages 399–406, 2010.
- Hengtao He, Chao-Kai Wen, Shi Jin, and Geoffrey Ye Li. Model-driven deep learning for mimo detection. *IEEE Transactions on Signal Processing*, 68:1702–1715, 2020.
- Kyle Henke, Michael Teti, Garrett Kenyon, Ben Migliori, and Gerd Kunde. Apples-to-spikes: The first detailed comparison of lasso solutions generated by a spiking neuromorphic processor. In *Proceedings of the International Conference on Neuromorphic Systems 2022*, pages 1–8, 2022.
- Gao Huang, Zhuang Liu, Laurens Van Der Maaten, and Kilian Q Weinberger. Densely connected convolutional networks. In *Proceedings of the IEEE conference on computer vision and pattern recognition*, pages 4700–4708, 2017.
- Aapo Hyvärinen and Erkki Oja. Independent component analysis: algorithms and applications. *Neural networks*, 13(4-5):411–430, 2000.
- Edward Kim, Darryl Hannan, and Garrett Kenyon. Deep Sparse Coding for Invariant Multimodal Halle Berry Neurons. In *2018 IEEE/CVF Conference on Computer Vision and Pattern Recognition*. IEEE, June 2018. doi: 10.1109/cvpr.2018.00122. URL <https://doi.org/10.1109/2Fcvpr.2018.00122>. Reporter: 2018 IEEE/CVF Conference on Computer Vision and Pattern Recognition.

- Martin Klaučo, Martin Kalúz, and Michal Kvasnica. Machine learning-based warm starting of active set methods in embedded model predictive control. *Engineering Applications of Artificial Intelligence*, 77:1–8, 2019.
- Alex Krizhevsky, Geoffrey Hinton, et al. Learning multiple layers of features from tiny images. 2009.
- Jana Lang, Martin Giese, Winfried Ilg, and Sebastian Otte. Generating sparse counterfactual explanations for multivariate time series. In *International Conference on Artificial Neural Networks (ICANN)*, pages 180–193. Springer Nature Switzerland, 2023. doi: 10.1007/978-3-031-44223-0_15.
- Bruno Lecouat, Jean Ponce, and Julien Mairal. Fully trainable and interpretable non-local sparse models for image restoration. In *Computer Vision—ECCV 2020: 16th European Conference, Glasgow, UK, August 23–28, 2020, Proceedings, Part XXII 16*, pages 238–254. Springer, 2020.
- Honglak Lee, Alexis Battle, Rajat Raina, and Andrew Y Ng. Efficient sparse coding algorithms. In *Advances in neural information processing systems*, pages 801–808, 2006.
- Honglak Lee, Chaitanya Ekanadham, and Andrew Ng. Sparse deep belief net model for visual area v2. *Advances in neural information processing systems*, 20, 2007.
- Wotao Li and Stanley Osher. Compressed sensing and matrix completion with uniform uncertainty principle. *SIAM Review*, 50(1):65–79, 2009.
- Sheng Y. Lundquist, Dylan M. Paiton, Peter F. Schultz, and Garrett T. Kenyon. Sparse encoding of binocular images for depth inference. In *2016 IEEE Southwest Symposium on Image Analysis and Interpretation (SSIAI)*. IEEE, March 2016. doi: 10.1109/ssiai.2016.7459190. URL <https://doi.org/10.1109%2Fssiai.2016.7459190>.
- Sheng Y. Lundquist, Melanie Mitchell, and Garrett T. Kenyon. Sparse Coding on Stereo Video for Object Detection. *arXiv preprint arXiv:1705.07144*, 2017. URL <https://arxiv.org/abs/1705.07144>.
- Julien Mairal, Francis Bach, Jean Ponce, and Guillermo Sapiro. Online dictionary learning for sparse coding. In *Proceedings of the 26th annual international conference on machine learning*, pages 689–696, 2009.
- Vishal Monga, Yuelong Li, and Yonina C Eldar. Algorithm unrolling: Interpretable, efficient deep learning for signal and image processing. *IEEE Signal Processing Magazine*, 38(2):18–44, 2021.
- Thanh T Nguyen, Charles Soussen, Jérôme Idier, and El-Hadi Djermoune. Np-hardness of ℓ_0 minimization problems: revision and extension to the non-negative setting. In *2019 13th International conference on Sampling Theory and Applications (SampTA)*, pages 1–4. IEEE, 2019.
- Bruno A Olshausen and David J Field. Emergence of simple-cell receptive field properties by learning a sparse code for natural images. *Nature*, 381(6583):607–609, 1996.
- Dylan M Paiton. *Analysis and applications of the Locally Competitive Algorithm*. University of California, Berkeley, 2019.
- Omkar M Parkhi, Andrea Vedaldi, Andrew Zisserman, and CV Jawahar. Cats and dogs. In *2012 IEEE conference on computer vision and pattern recognition*, pages 3498–3505. IEEE, 2012.
- Gavin Parpart, Sumedh Risbud, Garrett Kenyon, and Yijing Watkins. Implementing and benchmarking the locally competitive algorithm on the loihi 2 neuromorphic processor. In *Proceedings of the 2023 International Conference on Neuromorphic Systems*, pages 1–6, 2023.
- JH Rick Chang, Chun-Liang Li, Barnabas Póczos, BVK Vijaya Kumar, and Aswin C Sankaranarayanan. One network to solve them all—solving linear inverse problems using deep projection models. In *Proceedings of the IEEE International Conference on Computer Vision*, pages 5888–5897, 2017.
- Roberto Rigamonti, Matthew A. Brown, and Vincent Lepetit. Are sparse representations really relevant for image classification? In *CVPR 2011*. IEEE, June 2011. doi: 10.1109/cvpr.2011.5995313. URL <https://doi.org/10.1109%2Fcvpr.2011.5995313>.

- Christopher Rozell, Don Johnson, Richard Baraniuk, and Bruno Olshausen. Locally competitive algorithms for sparse approximation. In *2007 IEEE International Conference on Image Processing*, volume 4, pages IV–169. IEEE, 2007.
- Christopher J Rozell, Don H Johnson, Richard G Baraniuk, and Bruno A Olshausen. Sparse coding via thresholding and local competition in neural circuits. *Neural computation*, 20(10):2526–2563, 2008.
- Rajiv Sambharya, Georgina Hall, Brandon Amos, and Bartolomeo Stellato. Learning to warm-start fixed-point optimization algorithms. *arXiv preprint arXiv:2309.07835*, 2023.
- Jens Sjölund and Maria Bånkestad. Graph-based neural acceleration for nonnegative matrix factorization. *arXiv preprint arXiv:2202.00264*, 2022.
- Michael Teti, Garrett Kenyon, Ben Migliori, and Juston Moore. Lcanets: Lateral competition improves robustness against corruption and attack. In *International Conference on Machine Learning*, pages 21232–21252. PMLR, 2022.
- Robert Tibshirani. Regression Shrinkage and Selection Via the Lasso. *Journal of the Royal Statistical Society: Series B (Methodological)*, 58(1):267–288, January 1996. doi: 10.1111/j.2517-6161.1996.tb02080.x. URL <https://doi.org/10.1111%2Fj.2517-6161.1996.tb02080.x>. Publisher: Wiley.
- Cyril Vonesch and Michael Unser. A generalized forward-backward splitting algorithm for sparse signal recovery. *IEEE Transactions on Signal Processing*, 55(21):482–492, 2007.
- Jinxi Xiang, Yonggui Dong, and Yunjie Yang. Fista-net: Learning a fast iterative shrinkage thresholding network for inverse problems in imaging. *IEEE Transactions on Medical Imaging*, 40(5):1329–1339, 2021.
- Saining Xie, Ross Girshick, Piotr Dollár, Zhuowen Tu, and Kaiming He. Aggregated residual transformations for deep neural networks. In *Proceedings of the IEEE conference on computer vision and pattern recognition*, pages 1492–1500, 2017.
- Bo Xin, Yizhou Wang, Wen Gao, David Wipf, and Baoyuan Wang. Maximal sparsity with deep networks? In *Advances in Neural Information Processing Systems*, pages 4340–4348, 2016.
- Sergey Zagoruyko and Nikos Komodakis. Wide residual networks. *arXiv preprint arXiv:1605.07146*, 2016.
- Jian Zhang and Bernard Ghanem. Ista-net: Interpretable optimization-inspired deep network for image compressive sensing. In *Proceedings of the IEEE conference on computer vision and pattern recognition*, pages 1828–1837, 2018.
- Qingtian Zhang, Xiaolin Hu, Bo Hong, and Bo Zhang. A hierarchical sparse coding model predicts acoustic feature encoding in both auditory midbrain and cortex. *PLOS Computational Biology*, 15(2):e1006766, February 2019. ISSN 1553-7358. doi: 10.1371/journal.pcbi.1006766. URL <https://dx.plos.org/10.1371/journal.pcbi.1006766>.
- Ruijie Zhang, Jian Shen, Fushan Wei, Xiong Li, and Arun Kumar Sangaiah. Medical image classification based on multi-scale non-negative sparse coding. *Artificial Intelligence in Medicine*, 83:44–51, November 2017. ISSN 09333657. doi: 10.1016/j.artmed.2017.05.006. URL <https://linkinghub.elsevier.com/retrieve/pii/S0933365716306029>.
- Zheng Zhang, Yong Xu, Jian Yang, Xuelong Li, and David Zhang. A survey of sparse representation: algorithms and applications. *IEEE access*, 3:490–530, 2015.
- Zhonghao Zhang, Yipeng Liu, Jiani Liu, Fei Wen, and Ce Zhu. Amp-net: Denoising-based deep unfolding for compressive image sensing. *IEEE Transactions on Image Processing*, 30:1487–1500, 2020.

A Parameters for Training LCA on CIFAR

Table 2: LCA hyperparameters on CIFAR-10.

Hyperparameter	Value
Output neurons	100
Input neurons	3
Kernel size	9
Stride	2
Lambda	2.55
Tau	100
Eta	0.01
Lca iters	800
Pad	same
Nonneg	True
Transfer func	soft_threshold

Dictionary of Kernels trained on CIFAR Training Dataset

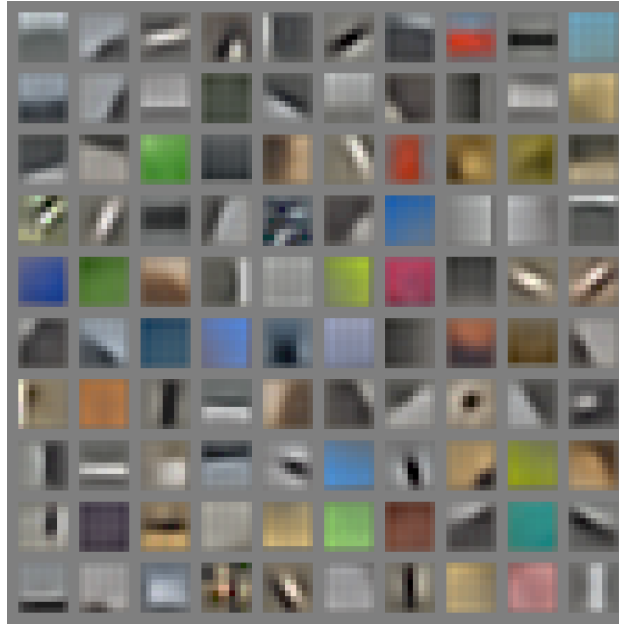


Figure 6: An exemplary dictionary of kernels obtained from training on the the CIFAR dataset

B WARP-CNN Architecture and Training hyper-parameters

Table 3: WARP-CNN Architecture

Layer	Type	Parameters	Output Shape
Common Layers			
Conv1	Conv2d	4, 512, kernel_size=5, stride=1, padding=2	(batch_size, 512, H, W)
BN1	BatchNorm2d	512	(batch_size, 512, H, W)
Conv2	Conv2d	512, 512, kernel_size=5, stride=1, padding=2	(batch_size, 512, H, W)
BN2	BatchNorm2d	512	(batch_size, 512, H, W)
Conv3	Conv2d	512, 512, kernel_size=3, stride=1, padding=1	(batch_size, 512, H, W)
BN3	BatchNorm2d	512	(batch_size, 512, H, W)
Conv4	Conv2d	512, 512, kernel_size=3, stride=1, padding=1	(batch_size, 512, H, W)
BN4	BatchNorm2d	512	(batch_size, 512, H, W)
Dropout	Dropout	p=0.3	(batch_size, 512, H, W)
Conv5	Conv2d	512, 512, kernel_size=3, stride=1, padding=1	(batch_size, 512, H, W)
BN5	BatchNorm2d	512	(batch_size, 512, H, W)
Conv6	Conv2d	512, 512, kernel_size=3, stride=1, padding=1	(batch_size, 512, H, W)
BN6	BatchNorm2d	512	(batch_size, 512, H, W)
AdjustChannels	Conv2d	512, 256, kernel_size=1	(batch_size, 256, H, W)
Downward Branch			
Conv_d1	Conv2d	512, 256, kernel_size=3, stride=1, padding=1	(batch_size, 256, H, W)
BN_d1	BatchNorm2d	256	(batch_size, 256, H, W)
Conv_d2	Conv2d	256, 256, kernel_size=3, stride=1, padding=1	(batch_size, 256, H, W)
BN_d2	BatchNorm2d	256	(batch_size, 256, H, W)
Conv_d3	Conv2d	256, 100, kernel_size=3, stride=2, padding=1	(batch_size, 100, H/2, W/2)
BN_d3	BatchNorm2d	100	(batch_size, 100, H/2, W/2)
Upward Branch			
Conv_u1	Conv2d	512, 256, kernel_size=3, stride=1, padding=1	(batch_size, 256, H, W)
BN_u1	BatchNorm2d	256	(batch_size, 256, H, W)
Conv_u2	Conv2d	256, 256, kernel_size=3, stride=1, padding=1	(batch_size, 256, H, W)
BN_u2	BatchNorm2d	256	(batch_size, 256, H, W)
Conv_u3	Conv2d	256, 100, kernel_size=3, stride=2, padding=1	(batch_size, 100, H/2, W/2)
BN_u3	BatchNorm2d	100	(batch_size, 100, H/2, W/2)

Table 5: Training and testing details for the CIFAR-10 dataset.

Detail	Description
Dataset	CIFAR-10 standard training and test splits
Data Transformation	ToTensor() Normalize(mean=[0.4914, 0.4822, 0.4465], std=[0.247, 0.243, 0.261])
Network Initialization	net.apply(lambda m: sparse_init(m, sparsity=0.9, std=0.01))
Sparse Initialization Function	<pre>def sparse_init(m, sparsity=0.9, std=0.01): if isinstance(m, (nn.Linear, nn.Conv2d)): with torch.no_grad(): sparse_weights = torch.randn(m.weight.size()) * std mask = torch.rand(m.weight.size()) > sparsity sparse_weights = sparse_weights * mask.float() m.weight = nn.Parameter(sparse_weights) if m.bias is not None: m.bias.data.zero_()</pre>
Optimizer	Adam Learning Rate = 0.0001 optimizer = torch.optim.Adam(net.parameters(), lr=0.0001)
Loss Function	custom_weighted_mse_loss_with_laplace_scale with non-zero weight scaling and Laplace-like scaling parameters. Non-zero weight: 1000.0, Laplace scale: 3.0.
Scaling of Target Activations	Target activations are scaled between 0 and 1 during training, and predicted targets are descaled during inference.
Validation Data	1% of the training data was used for validation

Table 4: Forward Pass of WARP CNN with Skip Connections

Step	Operation	Input	Output Shape
1	Conv1 + ReLU	x	(batch_size, 512, H, W)
2	BN1	Output of Step 1	(batch_size, 512, H, W)
3	Conv2 + ReLU	Output of Step 2	(batch_size, 512, H, W)
4	BN2	Output of Step 3	(batch_size, 512, H, W)
5	Conv3 + ReLU	Output of Step 4	(batch_size, 512, H, W)
6	BN3	Output of Step 5	(batch_size, 512, H, W)
7	Conv4 + ReLU	Output of Step 6	(batch_size, 512, H, W)
8	BN4	Output of Step 7	(batch_size, 512, H, W)
9	Dropout	Output of Step 8	(batch_size, 512, H, W)
10	Conv5 + ReLU	Output of Step 9	(batch_size, 512, H, W)
11	BN5	Output of Step 10	(batch_size, 512, H, W)
12	Dropout	Output of Step 11	(batch_size, 512, H, W)
13	Conv6 + ReLU	Output of Step 12	(batch_size, 512, H, W)
14	BN6	Output of Step 13	(batch_size, 512, H, W)
15	Dropout	Output of Step 14	(batch_size, 512, H, W)
16	AdjustChannels	Output of Step 15	(batch_size, 256, H, W)
Downward Branch			
17	Conv_d1 + ReLU	Output of Step 15	(batch_size, 256, H, W)
18	BN_d1	Output of Step 17	(batch_size, 256, H, W)
19	Conv_d2 + ReLU	Output of Step 18 + Output of Step 16	(batch_size, 256, H, W)
20	BN_d2	Output of Step 19	(batch_size, 256, H, W)
21	Conv_d3 + ReLU	Output of Step 20	(batch_size, FEATURES, H/2, W/2)
22	BN_d3	Output of Step 21	(batch_size, FEATURES, H/2, W/2)
Upward Branch			
23	Conv_u1 + ReLU	Output of Step 15	(batch_size, 256, H, W)
24	BN_u1	Output of Step 23	(batch_size, 256, H, W)
25	Conv_u2 + ReLU	Output of Step 24 + Output of Step 16	(batch_size, 256, H, W)
26	BN_u2	Output of Step 25	(batch_size, 256, H, W)
27	Conv_u3 + ReLU	Output of Step 26	(batch_size, FEATURES, H/2, W/2)
28	BN_u3	Output of Step 27	(batch_size, FEATURES, H/2, W/2)
29	Subtraction	Output of Step 22 - Output of Step 28	(batch_size, FEATURES, H/2, W/2)
30	Sigmoid	Output of Step 29	(batch_size, FEATURES, H/2, W/2)

C Training procedure for WARP-LCA

Algorithm 1 Training Dictionary, Encoding Data and Training CNN for WARP-LCA

```

1: Input: Dataset  $D$ , Number of epochs  $E$ , Initial  $\lambda$ , Increase factor  $f$ , Number of ISTA steps  $n$ 
2: Output: Trained Dictionary  $K$ , Encoded Dataset  $D'$ , Trained CNN
3: Initialize dictionary  $K$ 
4: for  $epoch = 1$  to  $E$  do
5:   for each sample in  $D$  do
6:     Perform  $n$  steps of ISTA with L1 sparsity (soft thresholding)
7:   end for
8:    $\lambda \leftarrow \lambda \times f$  ▷ Increase sparsity factor
9: end for
10: Encode dataset:
11: for each sample in  $D$  do
12:   Run LCA with hard thresholding
13:   Save activations to new dataset  $D'$ 
14: end for
15: Train CNN:
16: Initialize CNN
17: for each (input, label) in  $(D, D')$  do
18:   Train CNN on input to predict corresponding label
19: end for

```

D Training on Tiny ImageNet

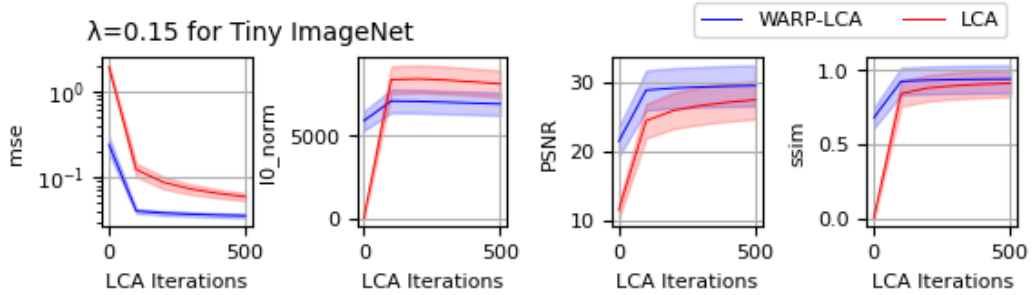


Figure 7: **Encoding Performance Comparison between WARP-LCA and LCA** The figure displays the performance metrics for WARP-LCA and LCA at $\lambda = 0.15$. The columns represent different metrics: Mean Squared Error (MSE), L0 Norm, Peak Signal-to-Noise Ratio (PSNR), and Structural Similarity Index (SSIM). For each plot, WARP-LCA and LCA performances are shown for comparison.

Table 6: Evaluation after 500 iterations on Tiny ImageNet dataset with $\lambda = 0.15$

Metric	Net Metrics Mean	LCA Metrics Mean
MSE	0.0353	0.0588
L_0 Norm	6946.22	8169.27
L_1 Norm	3411.67	2710.40
PSNR	29.46	27.38
SSIM	0.9377	0.9092

E Comparing WARP-LCA and LCA at higher sparsity levels

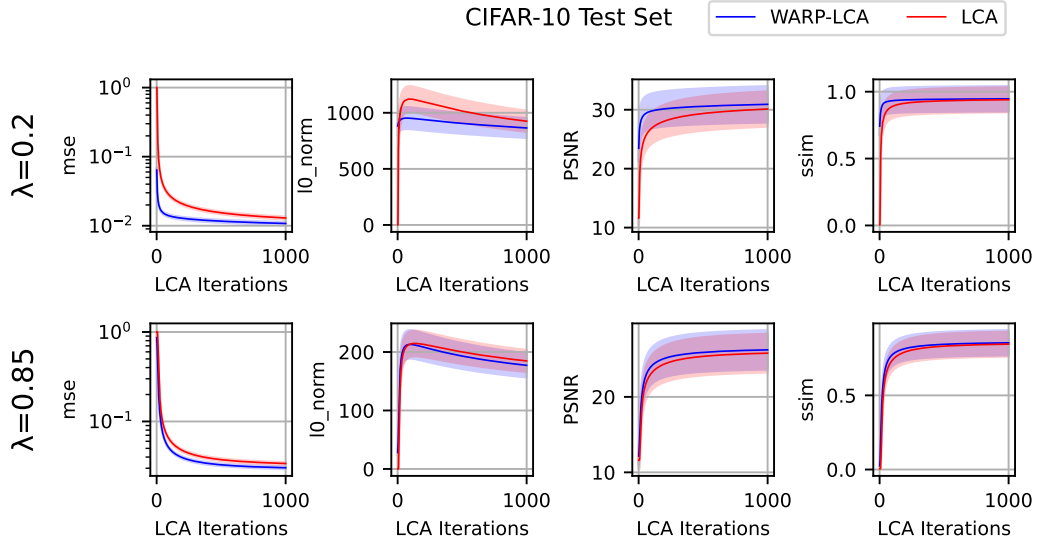


Figure 8: **Encoding Performance Comparison between WARP-LCA and LCA across Different Sparsity Levels.** The figure displays the performance metrics for WARP-LCA and LCA over two sparsity levels, $\lambda = 0.2$ and $\lambda = 0.85$. Each row corresponds to a different sparsity level. The first row represents $\lambda = 0.2$, while the second row represents $\lambda = 0.85$. The columns represent different metrics: Mean Squared Error (MSE), L_0 Norm, Peak Signal-to-Noise Ratio (PSNR), and Structural Similarity Index (SSIM). For each plot, WARP-LCA and LCA performances are shown for comparison.

F More Examples for Accumulated Aggregation Maps



Figure 9: **Larger Example of as shown in 5**

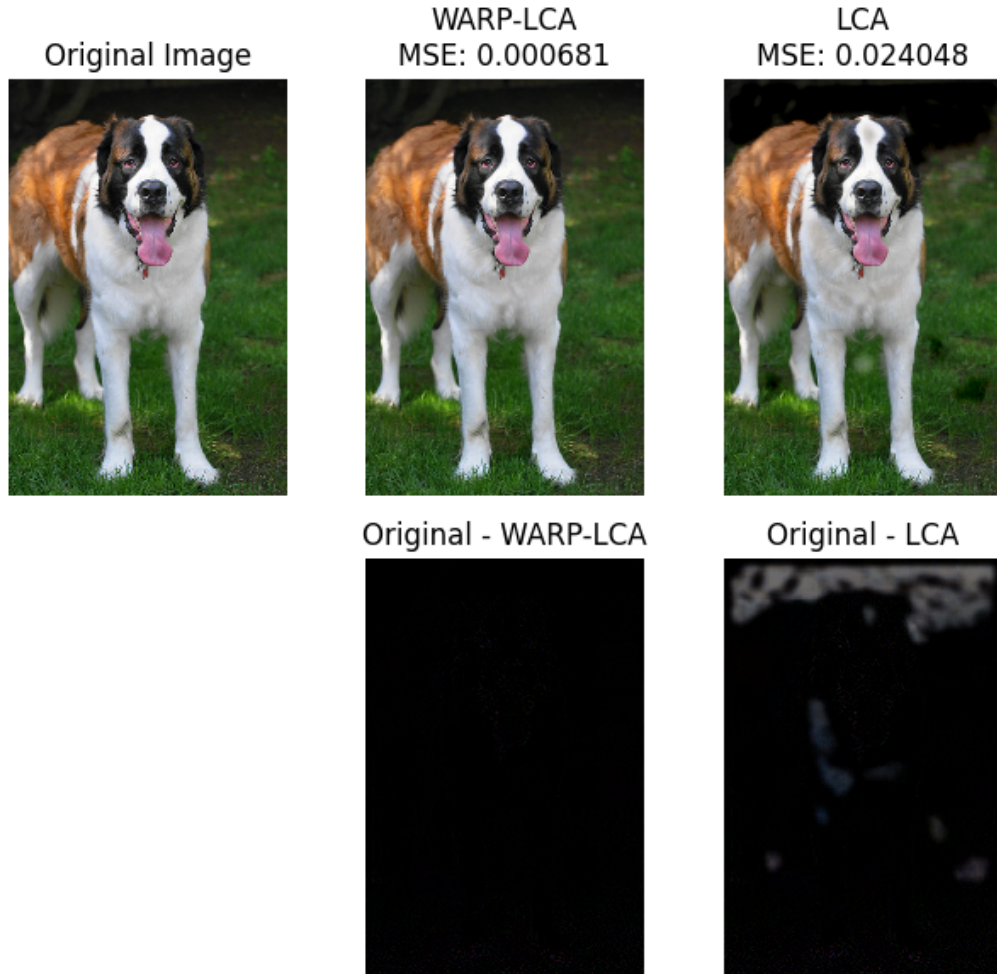


Figure 10: **Larger Example of as shown in 5.** Both WARP-LCA and LCA were executed for 1000 iterations to fully converge. Visibly, the LCA image has a worse reconstruction than the WARP-LCA image. It seems to struggle with very dark or bright areas of the original image as can be seen in the difference plot in the second row (subtraction of original image and respective LCA method).



Figure 11: **More Examples for Accumulated Aggregation Maps**

G Datasets

Table 7: Details of the datasets used in the study.

Dataset	License	Source	Authors	Link
CIFAR-10	MIT License	Canadian Institute For Advanced Research	Alex Krizhevsky, Geoffrey Hinton	https://www.cs.toronto.edu/~kriz/cifar.html
Oxford Pets	Creative Commons Attribution 4.0 International License	University of Oxford	O. M. Parkhi, A. Vedaldi, A. Zisserman	https://www.robots.ox.ac.uk/~vgg/data/pets/
Tiny ImageNet	Public Domain	Stanford University	Li-Jia Li, Fei-Fei Li	https://huggingface.co/datasets/zh-plus/tiny-imagenet

H Equivalence of LCA with Hard Thresholding to IHTA and Distinction from Matching Pursuit

H.1 Equivalence to IHTA with Hard Thresholding

We follow the example of the soft thresholding equivalence, given by Balavoine et al. [2015], to establish the equivalence between the Iterative Hard Thresholding Algorithm (IHTA) and LCA with hard thresholding, consider the IHTA update rule:

$$a^{(k+1)} = H_k \left(a^{(k)} + \eta \Phi^T (y - \Phi a^{(k)}) \right) \quad (7)$$

where $H_k(\cdot)$ is the hard thresholding operator that retains the top k largest (in magnitude) elements and sets the rest to zero.

Rewriting the LCA ODE with a discretization step size $\Delta t = \tau$:

$$\tau \frac{u[k+1] - u[k]}{\tau} = -u[k] + \Phi^T (y - \Phi a[k]) - (\Phi^T \Phi - I) a[k] \quad (8)$$

Assuming $u[k] = a[k]$ for the initial state, we have:

$$u[k+1] = a[k] + \Phi^T (y - \Phi a[k]) - (\Phi^T \Phi a[k] - a[k]) \quad (9)$$

Simplifying this:

$$u[k+1] = a[k] + \Phi^T (y - \Phi a[k]) \quad (10)$$

Then apply the hard thresholding operator:

$$a[k+1] = H_k(u[k+1]) \quad (11)$$

Comparing this with the IHTA update:

$$a^{(k+1)} = H_k \left(a^{(k)} + \eta \Phi^T (y - \Phi a^{(k)}) \right) \quad (12)$$

This shows that when assuming $u[k] = a[k]$ for the initial state, the update for $u[k+1]$ and applying the hard thresholding operator H_k leads to the same update rule as IHTA. Therefore, LCA with hard thresholding is equivalent to IHTA when the initial state assumption $u[k] = a[k]$ is used.

H.2 Distinction from Matching Pursuit with Hard Thresholding

Matching Pursuit (MP) employs a greedy, sequential strategy that iteratively selects the dictionary element with the highest correlation to the residual. The steps of MP are:

1. Initialize the residual $r^0 = y$ and set $a^0 = 0$.
2. For each iteration k :
 - Find the column Φ_j that best matches the residual: $j = \arg \max_i |\langle r^k, \Phi_i \rangle|$.
 - Update the coefficients: $a_j^{k+1} = a_j^k + \langle r^k, \Phi_j \rangle$.
 - Update the residual: $r^{k+1} = r^k - \langle r^k, \Phi_j \rangle \Phi_j$.

LCA with hard thresholding (ℓ_0 regularization) uses a parallel approach where all neurons compete simultaneously. The competition term $(I - \Phi^T \Phi) a^{(k)}$ in LCA introduces dynamics absent in MP. Thus, LCA with ℓ_0 regularization is not equivalent to Matching Pursuit.